

# A Hybrid Machine Learning Approach Using *LBP* Descriptor and *PCA* for Age-Related Macular Degeneration Classification in OCTA Images

Abdullah Alfahaid<sup>1,2,3</sup>, Tim Morris<sup>1</sup>, Tim Cootes<sup>4</sup>, Pearse A Keane<sup>2</sup>, Hagar Khalid<sup>2</sup>, Nikolas Pontikos<sup>2,5</sup>, Panagiotis Sergouniotis<sup>6</sup>, and Konstantinos Balaskas<sup>2</sup>

<sup>1</sup> School of Computer Science, The University of Manchester, Oxford Road, Manchester, M13 9PL, United Kingdom  
abdullah.alfahaid@manchester.ac.uk

<sup>2</sup> Moorfields Eye Hospital, 162 City Road, London, EC1V 2PD, United Kingdom

<sup>3</sup> College of Computer Science and Engineering at Yanbu, Taibah University, Medina, Kingdom of Saudi Arabia

<sup>4</sup> Centre for Imaging Sciences, The University of Manchester, Oxford Road, Manchester, M13 9PL, United Kingdom

<sup>5</sup> UCL Genetics Institute, University College London, Gower Street, London, WC1E 6BT, United Kingdom

<sup>6</sup> School of Biological Sciences, The University of Manchester, Oxford Road, Manchester, M13 9PL, United Kingdom

**Abstract.** We propose a novel hybrid machine learning approach for age-related macular degeneration (AMD) classification to support the automated analysis of images captured by optical coherence tomography angiography (OCTA). The algorithm uses a Rotation Invariant Uniform Local Binary Patterns (*LBP*) descriptor to capture local texture patterns associated with AMD and Principal Component Analysis (*PCA*) to decorrelate texture features. The analysis is performed on the entire image without targeting any particular area. The study focuses on four distinct groups, namely, healthy; neovascular AMD (an advanced stage of AMD associated with choroidal neovascularisation (CNV)); non-neovascular AMD (AMD without the presence of CNV) and secondary CNV (CNV due to retinal pathology other than AMD). Validation sets were created using a Stratified K-Folds Cross-Validation strategy for limiting the overfitting problem. The overall performance was estimated based on the area under the Receiver Operating Characteristic (ROC) curve (AUC). The classification was conducted as a binary classification problem. The best performance achieved with the SVM classifier based on the AUC score for: (i) healthy vs neovascular AMD was 100%, (ii) neovascular AMD vs non-neovascular AMD was 85%; (iii) CNV (neovascular AMD plus secondary CNV) vs non-neovascular AMD was 83%.

**Keywords:** Optical Coherence Tomography Angiography (OCTA) · Age-Related Macular Degeneration (AMD) · Texture Features

## 1 Motivation

Age-related macular degeneration (AMD) is a heterogeneous, multifactorial retinal condition and a leading cause of visual impairment in the elderly population [1, 2]. AMD predominantly affects the macula, the central part of the retina and it is clinically categorised into non-neovascular (or dry) AMD and neovascular (or wet) AMD [3]. The hallmark of dry AMD is drusen, focal deposits of extracellular debris located under the retina and the retinal pigment epithelium (RPE); retinal pigment epithelial abnormalities including atrophy are common. Wet AMD is characterised by the presence of a common, vision-threatening complication of AMD called choroidal neovascularisation (CNV); this involves the growth of abnormal blood vessels typically originating from the choroid (a layer of tissue located underneath the retina and RPE) and involving the macular area [3]. Dry AMD is the more common subtype and it is associated with gradual visual loss whereas wet AMD is linked to a more acute presentation [3]. Notably, wet AMD can be successfully treated with intravitreal injection. Early detection and management are key and timely diagnosis is linked to improved outcomes [4]. Significant effort and healthcare resources are therefore put to the early identification of CNV and to the differentiation between individuals with wet and dry forms of AMD.

Different medical imaging modalities have been developed to help with this task. A promising recently introduced technique is Optical Coherence Tomography Angiography (OCTA) which combines dye-free angiography and non-invasive volumetric three-dimensional imaging. This modality has advantages over the widely used Optical Coherence Tomography (OCT) as it enables detailed visualisation of the retinal and choroidal circulation. Furthermore, OCTA is fast and non-invasive unlike other established modalities, such as Fundus Fluorescein Angiography (FFA) and Indocyanine Green Angiography (ICG) [5, 6, 7]. Importantly, OCTA enables characterisation of moving and static elements of retinal and choroidal blood flow and it allows visualisation of CNV and other abnormalities that can help distinguish between dry and wet AMD.

OCTA produces clear images of the retinal vasculature in different retinal layers including the superficial inner retina, the deep inner retina, the outer retina and the choriocapillaris layers. The current clinical standard for detecting CNV and evaluating the efficacy of the treatments for wet AMD involves visually examining the textural appearance of images from each of these layers. However, this is not a trivial task given the significant amount of data in each OCTA scan, the pattern variations between individuals, and the fact that neovascular and non-neovascular areas may appear similar [8]. It is therefore not uncommon for clinicians to request a second opinion due to the difficulties involved in the interpretation process. Figure 1 demonstrates the texture appearance of the retinal vasculature in the various retinal layers in the OCTA images for different eye conditions. Images from eyes with no pathology, dry AMD and wet AMD are shown. The complexity of the blood vessels pattern variations between the different retinal layers can be appreciated.

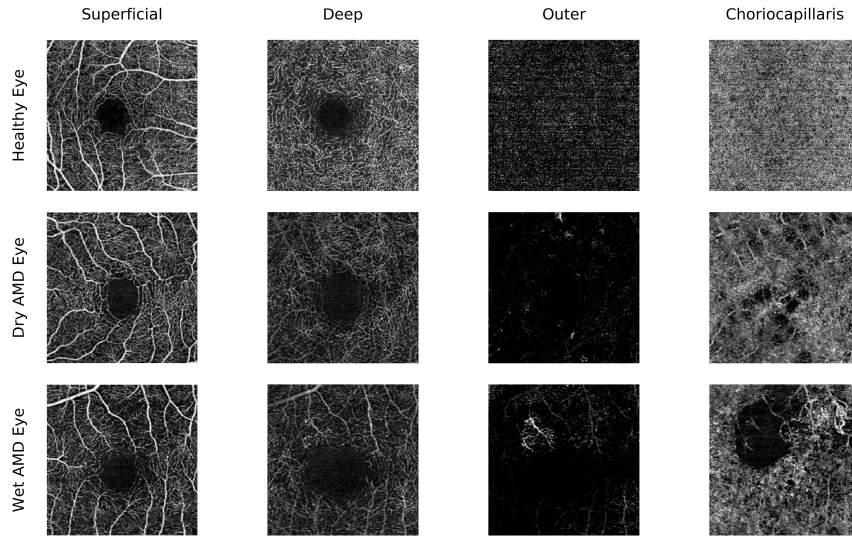


**Fig. 1.** The textural appearance of blood vessels network in the superficial inner retina, deep inner retina, outer retina and choriocapillaris layers in OCTA images. Each row illustrates a different eye condition from the various layers. The first shows a healthy eye, the second shows a dry AMD eye and the final row shows a wet AMD eye. It can be observed how the similarities appear in the patterns of the abnormalities in all layers for the dry and wet AMD eyes, while in some layers the patterns appear very similar, even in the healthy eye, namely the superficial inner and deep inner layers.

As seen in the previous figure, the texture of OCTA images is affected by AMD. Image texture is rich with very important information describing complex visual patterns that can be distinguished by colour, brightness, size or shape [9]. However, there is evidence to demonstrate that it is problematic for the human eye to recognise textural information which is related to higher-order statistics or to the spectral properties of an image [10]. Therefore, both quantifying the texture characteristics of OCTA images and building a predictive image classification algorithm that is capable of detecting the early stages of AMD is desirable. This could reduce the burden on ophthalmologists, remove the subjectivity due to personal interpretation and ensure a greater efficiency and reliability in the diagnosis process in daily clinical practice.

Image classification is an important component of computer-assisted medical diagnostic tools. Apart from an algorithm (based on Rotation Invariant Uniform Local Binary Patterns (*LBP*) as a texture descriptor) that was previously explored by our group [11], to the best of our knowledge, there has been no prior image classification work on AMD using OCTA images. The main contributions of the work undertaken are:

- The construction of new measurements that contribute the most to quantifying AMD presentation in OCTA images.

- The development of a novel hybrid machine learning approach for AMD classification with less redundant and misrepresentative texture features compared to our previous algorithm [11] as it has the additional advantageous capacity to decorrelate texture features by applying Principal Component Analysis (*PCA*).
- The application of our previous algorithm [11] and the new hybrid algorithm to a new much larger dataset provided by Moorfields Eye Hospital, which includes early stages of AMD disease.

## 2 Related Work

Numerous previous studies have focused on the development of methods to automate the analysis and detection of AMD in OCT or OCTA images. Most of these follow either an image segmentation-based or an image classification-based approach. The objective of image segmentation approaches is to partition the retinal vascular texture into disjunct regions. This includes the use of smoothing techniques as in [6], morphological operations as in [8] and manual-assistance by tracing the borders of the regions of interest as in [12]. Then, the images are labelled as healthy or AMD depending on either some measurements performed over the segmented regions or the visibility of the object of interest. This is in contrast with image classification, where the goal is to classify an unknown image into one of the pre-defined classes based on features derived from the image texture using machine learning and pattern recognition techniques. Many ways of deriving the features have been used, including handcrafted texture descriptors as in [13, 14, 15] or potentially the features learned using deep learning technologies as in [16, 17, 18].

When assessing image segmentation-based methods as clinical diagnostic tools for AMD detection in OCTA images, there are several limitations. Importantly, such approaches require an adequate image quality so that the abnormal blood vessel patterns are clearly visible; alternatively, the abnormalities can be difficult to segment. This problem is amplified by the fact that the measurements are likely to be derived from a deformed image texture structure due to the inclusion of pre-processing steps. These steps make use of morphological or smoothing operations as has occurred in [6] and [8] when part of the CNV, a key indicator of the presence of AMD, was excluded. Furthermore, the measurements may be influenced by human error/bias and often take considerable time when manual assistance is involved, as in [12]. To overcome the challenges associated with segmentation, an alternative path is to extract features from the whole image and use these features to build an image classification-based method.

While there are several image classification-based methods proposed, the vast majority were designed to be used on images produced from OCT rather than OCTA scans. However, OCT is not designed to produce images of the retinal vasculature and may fail to visualise/detect the abnormalities. What is more, handcrafted texture descriptor-based methods proposed in [13, 14, 15] are sensitive to noise such as image illumination variations and also include

complex operations and pre-processing steps to tackle image noise. However, that may change image details. On the other hand, it may be argued that deep learning-based methods using OCT images (including [16, 17, 18]) have greatly enhanced AMD detection performance despite the fact that a significant amount of training data was necessary to ensure that robust feature representations could be learned.

OCTA is an emerging imaging technique that enables visualisation of the retinal vasculature texture with an unprecedented level of detail. Given the recent introduction of robust OCTA imaging technologies only a limited amount of labelled training data is presently available. This and the complexity of OCTA images are important current limitations to the development of deep learning-based methods. Other issues with these methods include high computational complexity and memory requirements [19]. Moreover, they also present problems with the interpretation of outcomes due to the fact that the theoretical foundation is not well understood and the results are empirical [19].

### 3 Proposed Approach

The hybrid algorithm discussed in this paper follows the same pipeline of a previous algorithm reported by our group [11] but with an additional step of feature dimensionality reduction. Briefly, the new hybrid algorithm consists of three main steps. The first step is the texture feature extraction using the *LBP* descriptor to characterise all relevant variations in image texture patterns induced by AMD from the whole image. Subsequently, the feature dimensionality reduction step applies the *PCA*, which decorrelates the extracted features. Finally, there is a classification step, where the images are classified based on the new features represented by the *PCA*. Figure 2 shows a brief overview of the new hybrid algorithm pipeline for AMD classification.

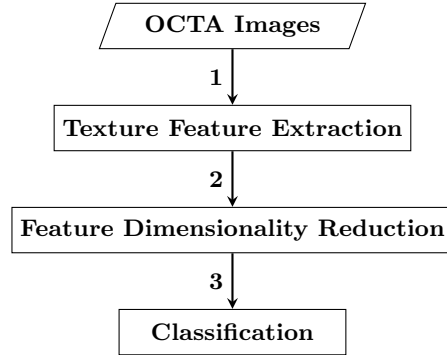


**Fig. 2.** Overview of the new analysis procedure for the hybrid classification algorithm. It begins with taking the OCTA images as an input, followed by feature extraction and dimensionality reduction respectively, and finally the classification.

### 3.1 Texture Feature Extraction

The study makes use of Rotation Invariant Uniform *LBP*, a handcrafted texture descriptor introduced by Ojala et al. [20]. Although there are several texture descriptors proposed in the literature, the choice of which one to use depends on the issues associated with the image texture to be measured and on how well the descriptor can cope with these issues [21]. Examples of common issues are the variations caused by rotation and illumination. Notably, OCTA image texture is affected by these changes [22]. Although the subjects' eyes are not purposefully rotated, there may be some orientation changes to the texture as the central, avascular region is orbited. Consequently, the main motivation of using the *LBP* in this study is that due to its various advantages (including ease of implementation) it can work effectively under limited resources. Also, it is capable of quantifying AMD in OCTA images while preserving the trade-off between two fundamental goals: (i) to provide a high-quality description with a balance between distinctiveness and robustness against the illumination and rotation changes; (ii) to have the lowest level of computational complexity.

To accurately measure the image texture using the *LBP*, the values of two important parameters need to be set up properly. The first parameter is the number of neighbouring points  $p$  spread on a circle and the second parameter is the radius  $r$  of the circle, which defines the length from the central point  $g_c$  to the neighbouring points  $g_n$ . The measurements are then derived by comparing a neighbouring point's  $g_n$  value, where  $n = (0, 1, 2, 3, \dots, p - 1)$ , against the central point  $g_c$  value generating a binary pattern. The *LBP* values for each pixel within each image are constructed according to the following equations:

$$LBP = \begin{cases} \sum_{n=0}^{n=p-1} S(g_n - g_c) & \text{if } u(LBP_{p,r}) \leq 2 \\ p + 1 & \text{Otherwise} \end{cases} \quad (1)$$

$$\text{Where } S(x) = \begin{cases} 1 & \text{if } x \geq 0 \\ 0 & \text{Otherwise} \end{cases}$$

$$u(LBP_{p,r}) = |S(g_{p-1} - g_c) - S(g_0 - g_c)| + \sum_{n=1}^{n=p-1} |S(g_n - g_c) - S(g_{n-1} - g_c)| \quad (2)$$

The  $u(LBP_{p,r})$  is a procedure to count the number of bitwise transitions and to consider the uniform binary patterns that have at most two transitions, 1/0 or 0/1. When measuring the image texture, the number of uniform binary patterns that can occur is  $p + 1$ . In this study, the whole OCTA image is processed without targeting any particular regions. Every image is described by a histogram with  $p + 2$  bins that calculates the number of occurrences of the uniform *LBP* values within each image, while the supplementary bin in the histogram is to calculate the non-uniform binary patterns that occurred. Then, the generated histogram will form the feature vector that represents each image.

### 3.2 Feature Dimensionality Reduction

In image classification problems, the high dimensional and highly correlated aspects of the feature vectors have a critical impact on the performance of the machine learning algorithm used for conducting the classification. Techniques that can significantly overcome these issues in an interpretable fashion while maintaining most of the important information in the feature space are desirable. One of the most popular and commonly utilised techniques for this task is Principal Component Analysis (*PCA*) [23]. *PCA* is a statistical technique that uses a linear transformation to convert a high number of correlated features into a lower number of linearly uncorrelated features, named the principal components that successively maximise variance [23]. The use of *PCA* in our new algorithm was mainly motivated by the fact that when we increase the number of points around a particular circle (when calculating the *LBP* values), the dimensionality of the feature vectors that represent each OCTA image also increases. Consequently, this is likely to increase the chance of having correlated and therefore redundant features; hence, *PCA* was applied, as it provides the following advantages:

- It makes the method less biased since it eliminates redundant texture features;
- It improves the accuracy of the method as it reduces the occurrence of misrepresentative texture features;
- It reduces the time taken for training the machine learning algorithm since it makes use of feature vectors of lower dimensionality.

In this step, the original dimensional feature vectors obtained from the OCTA images were reduced into lower dimensional feature vectors. These retained 95% of the variance which is a common percentage widely used when applying *PCA*.

### 3.3 Classification

Following the feature dimensionality reduction step, the newly constructed features are passed to a classifier for classification. Two different machine learning algorithms were tested in this work, namely K-Nearest Neighbour (KNN) and Support Vector Machine (SVM). The kernel type used for the SVM classifier is a linear kernel. The value of K neighbours for the KNN classifier was empirically set to one similar to our previous algorithm [11].

## 4 Evaluation

The hybrid algorithm described here and our previous algorithm [11] were evaluated based on their ability to distinguish between the various classes of images provided by Manchester Royal Eye Hospital and Moorfields Eye Hospital. The Manchester dataset included 23 healthy and 23 wet AMD samples. The Moorfields dataset included 166 wet AMD and 79 dry AMD cases; 25 secondary CNV

cases were also included. In these secondary CNV samples the neovascularisation was due to causes other than AMD. Both datasets include four different images of each eye captured from four retinal layers, namely the superficial inner retinal layer, the deep inner retinal layer, the outer retinal layer and choriocapillaris layer. Table 1 summarises the number of images used. The study makes use of two-dimensional angiogram greyscale images captured from a 3x3 mm field of view and utilises all the pre-segmented images through the retinal layers by the default setting of the OCTA scan. This is because we wanted to avoid the additional complexity of manually segmenting the images. The addition of such a step would make the algorithm less user-friendly and would probably introduce bias.

**Table 1.** Summary for the number of images used in this study.

Hospital	Classes	Retinal Layers				All Layers
		Choriocapillaris	Outer	Deep	Superficial	
Manchester	healthy	23	23	23	23	92
	wet AMD	23	23	23	23	92
Moorfields	wet AMD	166	166	166	166	664
	non-CNV (dry AMD)	79	79	79	79	316
	secondary CNV	25	25	25	25	100

#### 4.1 Evaluation Setup and Criteria

The classification was performed on each separate layer and in all layers combined as a binary classification problem. The motivations for performing the classification this way (on each separate layer) are to identify the predictive layer that has most information describing the abnormalities, and (in all layers combined) to investigate how well the algorithms operate on classifying the various layers at once by throwing all layers together. The classification was conducted as follows:

- I healthy vs wet AMD for the Manchester dataset;
- II wet AMD vs dry AMD for the Moorfields dataset;
- III CNV (wet AMD plus secondary CNV) vs non-CNV (dry AMD) for the Moorfields dataset.

As the Moorfields dataset is imbalanced and all classes are important for us to detect, the following evaluation strategies for both algorithms were conducted on both datasets:

- Use the Stratified K-Folds Cross-Validation strategy to split the data into training and testing sets creating stratified folds; this means each fold is created by preserving the number of samples of each class. This is to ensure a consistent predictive performance for both algorithms and limitation of the overfitting problem.

- Use the Receiver Operating Characteristic (ROC) curve and compute the area under the curve (AUC). This is to provide equal weight for both classes in our binary classification problem.

These would give an accurate measure of insight into overall performance as well as ensuring enhanced validation for both algorithms.

## 4.2 Example Results

The performance of both algorithms was compared based on their AUC scores. The results are obtained by empirically choosing the same values of *LBP* parameters  $p$  and  $r$  that were used in our previous algorithm [11]. Two classifiers were tested on both approaches and the following two tables provide a comparison between their results. Table 2 provides the results of the SVM classifier and Table 3 shows the results of the KNN classifier. In both tables, the new hybrid algorithm is denoted as “Hybrid algorithm” while our previous algorithm [11] is denoted as “Previous algorithm”.

**Table 2.** Classification results using both approaches with SVM classifier.

Algorithm	Binary Classification	Retinal Layers				All Layers
		Choriocapillaris	Outer	Deep	Superficial	
Hybrid algorithm	healthy vs wet AMD	<b>100% ± 0</b>	99% ± 1	98% ± 3	95% ± 5	96% ± 2
	wet AMD vs dry AMD	83% ± 2	<b>85% ± 3</b>	80% ± 4	75% ± 3	78% ± 4
	CNV vs non-CNV	81% ± 3	<b>83% ± 1</b>	76% ± 2	69% ± 4	76% ± 2
Previous algorithm	healthy vs wet AMD	<b>100% ± 0</b>	96% ± 1	96% ± 3	91% ± 3	92% ± 3
	wet AMD vs dry AMD	81% ± 2	<b>83% ± 3</b>	79% ± 4	71% ± 2	75% ± 3
	CNV vs non-CNV	80% ± 3	<b>82% ± 3</b>	72% ± 4	67% ± 5	74% ± 3

**Table 3.** Classification results using both approaches with KNN classifier.

Algorithm	Binary Classification	Retinal Layers				All Layers
		Choriocapillaris	Outer	Deep	Superficial	
Hybrid algorithm	healthy vs wet AMD	<b>100% ± 0</b>	99% ± 1	96% ± 2	93% ± 5	96% ± 3
	wet AMD vs dry AMD	81% ± 3	<b>84% ± 4</b>	75% ± 5	73% ± 2	75% ± 4
	CNV vs non-CNV	80% ± 4	<b>81% ± 5</b>	73% ± 3	68% ± 4	73% ± 2
Previous algorithm	healthy vs wet AMD	<b>100% ± 0</b>	98% ± 2	95% ± 4	90% ± 4	90% ± 2
	wet AMD vs dry AMD	<b>80% ± 1</b>	78% ± 4	71% ± 4	70% ± 3	71% ± 2
	CNV vs non-CNV	79% ± 4	<b>79% ± 3</b>	70% ± 5	66% ± 3	70% ± 1

The construction of discriminative features has a critical role in the performance of machine learning algorithms. This is due to the fact that when using misleading or highly correlated texture features, even with the use of the most sophisticated classifiers, attaining the desired performance level will not be possible. The preliminary results in Tables 2 and 3 show that the new hybrid algorithm is robust against image noise and quality due to patient motion or illumination

changes as compared to our previously reported algorithm [11]. This was confirmed by challenging two different classifiers, namely the SVM and KNN. Furthermore, the SVM classifier generally performs better than the KNN classifier on both algorithms. Moreover, the initial results of our classification algorithms show that the most predictable layers are the choriocapillaris and outer retinal layers.

## 5 Conclusion and Future Work

This paper reports a hybrid algorithm for AMD classification in OCTA images by combining the *LBP* descriptor with *PCA*. The *LBP* is responsible for capturing the local textural features from the OCTA images while the *PCA* is applied for eliminating the misrepresentative texture features. The algorithm is capable of capturing all related image variations induced by AMD as analysis is performed on the entire image. The results achieved so far have suggested that the proposed hybrid algorithm may be clinically useful for AMD classification in OCTA images. Deep learning methods might have superior performance, but the size of the dataset currently available is too small to investigate them.

Future work exploring the performance of deep learning methods in similar tasks would be of interest. To enable this, the collection of carefully curated data will be required. Data augmentation techniques to increase the number of images are generally inappropriate, since in this case they will distort the data in undesirable ways. Testing the presented and other algorithms on more complex tasks would also be of interest. Specifically, it would be clinically valuable to be able to distinguish variations in AMD in the same patient, namely active CNV (which requires treatment) from inactive CNV (which can be observed).

## References

1. J. M. Colijn, G. H. Buitendijk, E. Prokofyeva, D. Alves, M. L. Cachulo, A. P. Khawaja, A. Cougnard-Gregoire, B. M. Merle, C. Korb, M. G. Erke, *et al.*, “Prevalence of Age-Related Macular Degeneration in Europe: The Past and the Future,” *Ophthalmology*, vol. 124, pp. 1753–1763, 12 2017.
2. R. R. Bourne, J. B. Jonas, S. R. Flaxman, J. Keeffe, J. Leasher, K. Naidoo, M. B. Parodi, K. Pesudovs, H. Price, R. A. White, *et al.*, “Prevalence and causes of vision loss in high-income countries and in Eastern and Central Europe: 1990-2010,” *Br J Ophthalmol*, vol. 98, pp. 629–638, May 2014.
3. P. Mitchell, G. Liew, B. Gopinath, and T. Y. Wong, “Age-related macular degeneration,” *Lancet*, vol. 392, pp. 1147–1159, 09 2018.
4. H. Mehta, A. Tufail, V. Daien, A. Y. Lee, V. Nguyen, M. Ozturk, D. Barthelmes, and M. C. Gillies, “Real-world outcomes in patients with neovascular age-related macular degeneration treated with intravitreal vascular endothelial growth factor inhibitors,” *Prog Retin Eye Res*, vol. 65, pp. 127–146, 07 2018.
5. Y. Jia, S. T. Bailey, T. S. Hwang, S. M. McClintic, S. S. Gao, M. E. Pennesi, C. J. Flaxel, A. K. Lauer, D. J. Wilson, J. Hornegger, *et al.*, “Quantitative optical coherence tomography angiography of vascular abnormalities in the living human eye,” *Proceedings of the National Academy of Sciences*, p. 201500185, 2015.

6. Y. Jia, S. T. Bailey, D. J. Wilson, O. Tan, M. L. Klein, C. J. Flaxel, B. Potsaid, J. J. Liu, C. D. Lu, M. F. Kraus, *et al.*, “Quantitative optical coherence tomography angiography of choroidal neovascularization in age-related macular degeneration,” *Ophthalmology*, vol. 121, no. 7, pp. 1435–1444, 2014.
7. T. E. De Carlo, A. Romano, N. K. Waheed, and J. S. Duker, “A review of optical coherence tomography angiography (octa),” *International Journal of Retina and Vitreous*, vol. 1, no. 1, p. 5, 2015.
8. L. Liu, S. S. Gao, S. T. Bailey, D. Huang, D. Li, and Y. Jia, “Automated choroidal neovascularization detection algorithm for optical coherence tomography angiography,” *Biomedical optics express*, vol. 6, no. 9, pp. 3564–3576, 2015.
9. P. Simon and V. Uma, “Review of texture descriptors for texture classification,” in *Data Engineering and Intelligent Computing*, pp. 159–176, Springer, 2018.
10. G. D. Tourassi, “Journey toward computer-aided diagnosis: role of image texture analysis,” *Radiology*, vol. 213, no. 2, pp. 317–320, 1999.
11. A. Alfahaid and T. Morris, “An automated age-related macular degeneration classification based on local texture features in optical coherence tomography angiography,” in *Annual Conference on Medical Image Understanding and Analysis*, pp. 189–200, Springer, 2018.
12. E. Talisa, M. A. Bonini Filho, A. T. Chin, M. Adhi, D. Ferrara, C. R. Bauml, A. J. Witkin, E. Reichel, J. S. Duker, and N. K. Waheed, “Spectral-domain optical coherence tomography angiography of choroidal neovascularization,” *Ophthalmology*, vol. 122, no. 6, pp. 1228–1238, 2015.
13. P. P. Srinivasan, L. A. Kim, P. S. Mettu, S. W. Cousins, G. M. Comer, J. A. Izatt, and S. Farsiu, “Fully automated detection of diabetic macular edema and dry age-related macular degeneration from optical coherence tomography images,” *Biomedical optics express*, vol. 5, no. 10, pp. 3568–3577, 2014.
14. Y. Wang, Y. Zhang, Z. Yao, R. Zhao, and F. Zhou, “Machine learning based detection of age-related macular degeneration (amd) and diabetic macular edema (dme) from optical coherence tomography (oct) images,” *Biomedical optics express*, vol. 7, no. 12, pp. 4928–4940, 2016.
15. Y. Sun, S. Li, and Z. Sun, “Fully automated macular pathology detection in retina optical coherence tomography images using sparse coding and dictionary learning,” *Journal of biomedical optics*, vol. 22, no. 1, p. 016012, 2017.
16. M. Treder, J. L. Laueremann, and N. Eter, “Automated detection of exudative age-related macular degeneration in spectral domain optical coherence tomography using deep learning,” *Graefe’s Archive for Clinical and Experimental Ophthalmology*, vol. 256, no. 2, pp. 259–265, 2018.
17. T. Schlegl, S. M. Waldstein, H. Bogunovic, F. Endstraßer, A. Sadeghipour, A.-M. Philip, D. Podkowinski, B. S. Gerendas, G. Langs, and U. Schmidt-Erfurth, “Fully automated detection and quantification of macular fluid in oct using deep learning,” *Ophthalmology*, vol. 125, no. 4, pp. 549–558, 2018.
18. C. S. Lee, D. M. Baughman, and A. Y. Lee, “Deep learning is effective for classifying normal versus age-related macular degeneration oct images,” *Ophthalmology Retina*, vol. 1, no. 4, pp. 322–327, 2017.
19. Y. Guo, Y. Liu, A. Oerlemans, S. Lao, S. Wu, and M. S. Lew, “Deep learning for visual understanding: A review,” *Neurocomputing*, vol. 187, pp. 27–48, 2016.
20. T. Ojala, M. Pietikainen, and T. Maenpaa, “Multiresolution gray-scale and rotation invariant texture classification with local binary patterns,” *IEEE Transactions on pattern analysis and machine intelligence*, vol. 24, no. 7, pp. 971–987, 2002.

21. T. Ojala and M. Pietikainen, "Texture classification," 2001. [http://homepages.inf.ed.ac.uk/rbf/CVonline/LOCAL\\_COPIES/OJALA1/texclas.htm](http://homepages.inf.ed.ac.uk/rbf/CVonline/LOCAL_COPIES/OJALA1/texclas.htm), Accessed: 01-Jan-2019.
22. R. F. Spaide, J. G. Fujimoto, and N. K. Waheed, "Image artifacts in optical coherence angiography," *Retina (Philadelphia, Pa.)*, vol. 35, no. 11, p. 2163, 2015.
23. I. Jolliffe, "Principal component analysis," in *International encyclopedia of statistical science*, pp. 1094–1096, Springer, 2011.